Supporting information

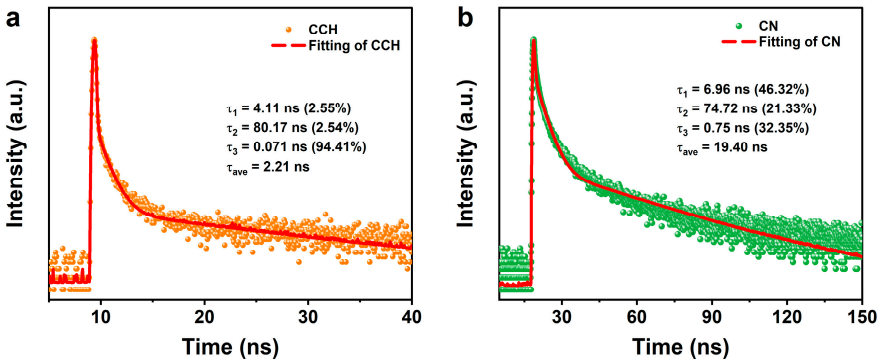

Figure S1. Time-resolved PL decay spectra of (a) CCH and (b) CN.

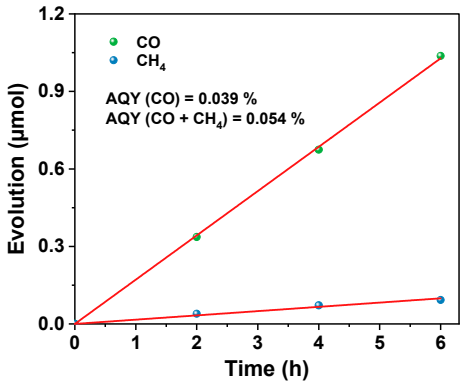

Figure S2. Time-dependent photocatalytic CO_2 reduction performance of CCH/CN at 420 nm band-pass filter irradiation and corresponding apparent quantum yield.

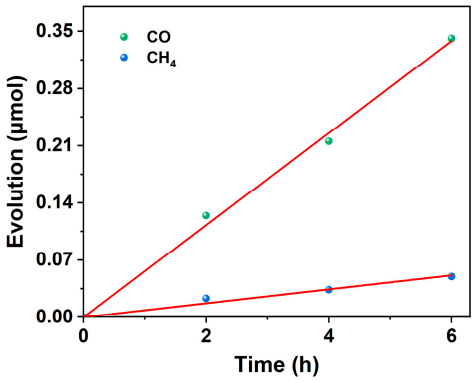

Figure S3. Time-dependent photocatalytic CO_2 reduction performance of CCH/CN at 500 nm band-pass filter irradiation.

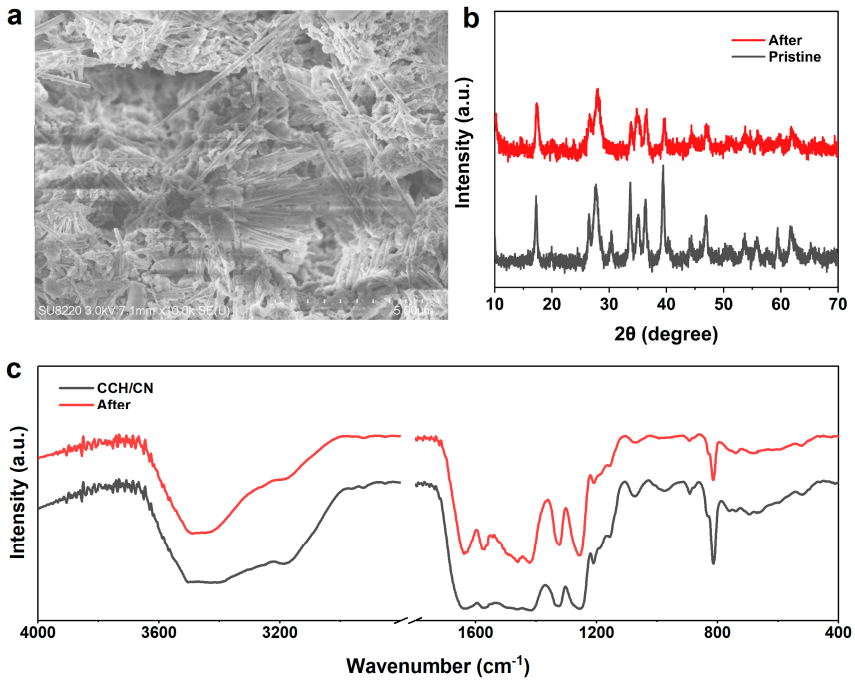

Figure S4. (a) SEM image of the as-prepared CCH/CN after durability test. (b) XRD pattern and (c) FTIR spectra of the as-prepared CCH/CN before and after durability test.

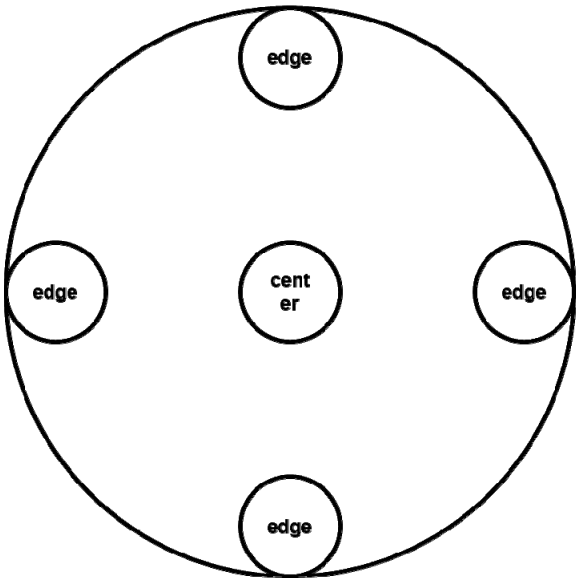

Figure S5. The measured sites of light intensity.

Table S1. The assignments of IR active modes measured at room temperature.

IR modes	Wavenumber (cm^{-1})			
	CCH	**CN**	**CCH/CN**	**Mix**
N-H	--	3432	3432	3432
Tri-s-triazine ring	--	1249	1256	1255
	--	1321	1326	1324
	--	1413	1420	1419
CO_3^{2-}	686	--	695	686
	968	--	977	977

Table S2. The assignments of Raman active modes of the CCH, CN, Mix and CN/CCH measured at room temperature.

Raman modes	Raman shifts (cm^{-1})			
	CCH	**CN**	**CCH/CN**	**Mix**
CO_3^{2-}	691	--	691	691
	1087	--	1087	1087
Co-O	481	--	483	482
Tri-s-triazine ring	--	452	454	452
	--	472	470	471
	--	487	484	485
	--	707	706	706
	--	769	768	767
	--	1117	1115	1116
	--	1154	1151	1153
	--	1216	1214	1215
	--	1234	1232	1233

Table S3. Relative ratio of C-C=N, N-$(C)_3$, and C-NH_3 determined by N 1s XPS spectra.

Samples	C-C=N	N-$(C)_3$	C-NH_3
CN	42.8%	41.7%	15.5%
CCH/CN	55.0%	35.2%	9.8%

Table S4. Summary of the photocatalytic CO evolution performance of some C_3N_4-based catalysts.

Samples	Light source	Product	Activity ($\mu mol\ g^{-1}\ h^{-1}$)	CO product selectivity	Ref.
CCH/CN	300 W Xe lamp (20.4 mW cm^{-2})	CO	19.65	96.6%	This work
		CH_4	0.69		
WO_3/C3N4	300 W Xe lamp	CO	9.4	78.3%	[1]
		CH_4	2.6		
g-C_3N_4/ZnNCN @ZIF-8	300 W Xe lamp	CO	0.47	56.0%	[2]
		CH_4	0.37		
$BiVO_4$/Ni_2P/g-C_3N_4	300 W Xe lamp	CO	6.40	98.3%	[3]
		CH_4	0.11		
TiO_2/C_3N_4/Ti_3C_2 MXene	350 W Xe lamp	CO	4.39	78.5%	[4]
		CH_4	1.20		
Co-MOF/g-C_3N_4	300 W Xe lamp (λ > 420 nm)	CO	6.75	55.2%	[5]
		CH_4	5.47		
g-C_3N_4/$BiVO_4$	300 W Xe lamp (λ > 420 nm)	CO	5.19	53.2%	[6]
		CH_4	4.57		
ZnTP/CN	300W Xe lamps (λ > 400 nm)	CO	19.4	95.8%	[7]
		CH_4	0.85		
TCPP-C_3N_4	300W Xe lamps (λ > 420 nm)	CO	16.8	96.3%	[8]
		CH_4	0.64		
$CuInS_2$/Au/g-	300 W Xe lamp	CO	19.46	94.3%	[9]

C_3N_4	(λ > 400 nm)	CH_4	1.18		
p-C_3N_4/$InVO_4$	300 W Xe lamp (λ > 400 nm)	CO	14.05	88.2%	[10]
		CH_4	1.88		
Bi_3O_4Cl/g-C_3N_4	300 W Xe lamp ($\lambda \geq 400$ nm)	CO	6.6	77.6%	[11]
		CH_4	1.9		

References:

1. Song, Z.; Chen, Q.; Sun, Z.; Chang, K.; Xie, Z.; Kuang, Q. Constructing Z-scheme WO_3/C_3N_4 heterojunctions with an enlarged internal electric field and accelerated water oxidation kinetics for robust CO_2 photoreduction. *J. Mater. Chem. A* **2024**, *12*, 14426-14436.

2. Xie, Y.; Zhuo, Y.; Liu, S.; Lin, Y.; Zuo, D.; Wu, X.; Li, C.; Wong, P. K. Ternary g-C_3N_4/ZnNCN@ZIF-8 Hybrid Photocatalysts with Robust Interfacial Interactions and Enhanced CO_2 Reduction Performance. *Solar RRL* **2020**, *4*, 1900440.

3. Hu, C.; Cao, J.; Jia, X.; Sun, H.; Lin, H.; Chen, S. Difunctional Ni_2P decorated novel Z-scheme $BiVO_4$/g-C_3N_4 heterojunction for achieving highly efficient CO_2 reduction and tetracycline oxidation. *Appl. Catal. B: Environ.* **2023**, *337*, 122957.

4. He, F.; Zhu, B.; Cheng, B.; Yu, J.; Ho, W.; Macyk, W. 2D/2D/0D $TiO_2/C_3N_4/Ti_3C_2$ MXene composite S-scheme photocatalyst with enhanced CO_2 reduction activity. *Appl. Catal. B: Environ.* **2020**, *272*, 119006.

5. Chen, Q.; Li, S.; Xu, H.; Wang, G.; Qu, Y.; Zhu, P.; Wang, D. Co-MOF as an electron donor for promoting visible-light photoactivities of g-C_3N_4 nanosheets for CO_2 reduction. *Chinese J. Catal.* **2020**, *41*, 514-523.

6. Lu, M.; Li, Q.; Zhang, C.; Fan, X.; Li, L.; Dong, Y.; Chen, G.; Shi, H. Remarkable photocatalytic activity enhancement of CO_2 conversion over 2D/2D g-C_3N_4/$BiVO_4$ Z-scheme heterojunction promoted by efficient interfacial charge transfer. *Carbon* **2020**, *160*, 342-352.

7. Jia, Z.; Xiao, Y.; Guo, S.; Xiong, L.; Yu, P.; Lu, T.; Song, R. Porphyrin Supramolecular Nanoassembly/C_3N_4 Nanosheet S-Scheme Heterojunctions for Selective Photocatalytic CO_2 Reduction toward CO. *ACS Appl. Mater. Interfaces* **2023**, *15*, 47070-47080.

8. Chen, Q.; Zhang, Y.; You, E.; Jiang, Q.; Chen, X.; Wang, Y.; Song, Z.; Chang, K.; Xie, Z.; Kuang, Q. Accelerated Water Oxidation Kinetics Triggered by Supramolecular Porphyrin Nanosheet for Robust Visible-Light-Driven CO_2 Reduction. *Small* **2022**, *18*, 2204924.

9. Ye, W.; Hu, J.; Hu, X.; Zhang, W.; Ma, X.; Wang, H. Rational Construction of Z-Scheme $CuInS_2$/Au/g-C_3N_4 Heterostructure: Experimental Results and Theoretical Calculation. *ChemCatChem* **2019**, *11*, 6372-6383.

10. Wang, L.; Chen, D.; Miao, S.; Chen, F.; Guo, C.; Ye, P.; Ning, J.; Zhong, Y.; Hu, Y. Nitric

acid-assisted growth of $InVO_4$ nanobelts on protonated ultrathin C_3N_4 nanosheets as an S-scheme photocatalyst with tunable oxygen vacancies for boosting CO_2 conversion. *Chem. Eng. J.* **2022**, *434*, 133867.

11. Xu, Y.; Jin, X.; Ge, T.; Xie, H.; Sun, R.; Su, F.; Li, X.; Ye, L. Realizing efficient CO_2 photoreduction in Bi_3O_4Cl: Constructing van der Waals heterostructure with g-C_3N_4. *Chem. Eng. J.* **2021**, *409*, 128178.